

Systematic Study of Incomplete Fusion Dynamics with Various Entrance Channel Parameters

Rahbar Ali^{a*}, D Singh^b, Suhail A Tali^c, Harish Kumar^d, Mohd Asif Khan^a, Nitin Sharma^b, Jagat Jyoti Mohapatra^b,
Lupteindu Chhura^b, M Afzal Ansari^c, M H Rashid^f, R Guin^f, S K Das^f, Rakesh Kumar^g & S Muralithar^g

^aDepartment of Physics, GF (P. G.) College, Shahjahanpur 242 001, India

^bCentre for Applied Physics, Central University of Jharkhand, Ranchi 835 205, India

^cDepartment of Physics, Central University of Kashmir, Ganderbal, Jammu & Kashmir 191 131, India

^dDepartment of Physics, Nims University of Rajasthan, Jaipur 303 121, India

^eDepartment of Physics, Aligarh Muslim University, Aligarh 202 002, India

^fVariable Energy Cyclotron Centre, 1/AF Bidhan Nagar, Kolkata 700 064, India

^gInter University Accelerator Centre, New Delhi 110 067, India

Received 19 May 2023; accepted 10 July 2023

The present work aims to differentiate the contributions of complete fusion (CF) and incomplete fusion (ICF) components by the measurement and analysis of the forward recoil range distribution of ²⁰Ne projectile with ¹⁵⁹Tb target nucleus. The recoil catcher technique has been employed for the identification of residues populated in the collision of ²⁰Ne-ion beam at projectile energy ~8.2 MeV per nucleon. The result obtained from the study suggests that the complete fusion reaction occurs with complete momentum transfer, which leads to large recoil ranges of the reaction products. However, the presence of incomplete fusion, resulting from the break-up of ²⁰Ne into ¹⁶O + ⁴He, ¹²C + ⁸Be, and/or ⁸Be + ¹²C, involves partial momentum transfer, leading to small recoil ranges where one of the fragments undergoes fusion with the ¹⁵⁹Tb target nucleus. Moreover, upon analyzing the data, the ICF fraction (F_{ICF}) has been estimated and compared with literature data as a function of various entrance channel parameters, namely Mass-asymmetry (μ_{MA}), Coulomb factor ($Z_P Z_T$), Deformation parameter (β_2) and $Z_P Z_T \times \beta_2$. The outcomes offer valuable insights into the entrance channel parameters that influence incomplete fusion dynamics. Additionally, a new entrance channel parameter called Zeta (ζ) was introduced to investigate the combined effect of μ_{MA} and $Z_P Z_T$.

Keywords: Complete and Incomplete fusion reactions; Recoil range distribution measurements; Foil Activation technique

1 Introduction

The phenomenon of incomplete fusion (ICF) holds paramount importance in the realm of fusion reactions. Given its substantial contribution to the total reaction cross-section, it serves as a valuable tool in comprehending the comprehensive reaction dynamics. Moreover, ICF is associated with the nascent phase of nuclear interaction, thus acting as a crucial intermediary in shedding light on the transition from the one-body mean-field behaviour at lower energies to the advent of two-body nucleon-nucleon interactions at higher energies. Fusion reactions based on complete fusion (CF) and/or ICF have applications spanning from super heavy elements (SHEs) synthesis to important radioisotope production¹⁻³. ICF reaction plays a significant role where projectiles break up into fragments. The disintegration takes place at energy

above the Coulomb barrier. Essentially, in CF, the projectile completely amalgamates into the target nucleus, where the entire linear momentum is transferred to the target nucleus. While in an ICF reaction, the projectile partially fuses with the target nucleus. As a result, partial momentum transfer takes place. In the early 1960s, Britt and Quinton⁴ were pioneers in the study of ICF reaction dynamics. By means of their experimental work, they successfully observed the rapid movement of α -particles in the reaction of ¹²C, ¹⁴N, and ¹⁶O projectiles with ²⁰⁹Bi and ¹⁹⁷Au targets. This ground-breaking research paved the way for further exploration into the intricacies of these reactions and their potential applications. Subsequently, Inamura *et al.*⁵, Glain *et al.*⁶, Parker *et al.*⁷ & Gomes *et al.*⁸ furthermore observed the ICF reaction in various heavy ion-induced reactions. The studies available in the literature^{9, 10} showed noticeable ICF contribution in α -emission products.

*Corresponding author: (E-mail: rahbara@gmail.com)

Several models, like BUF model¹¹, SUM-RULE model¹² etc., have been proposed to understand the reaction dynamics of the break-up fusion process. These models could not explain the ICF data at energies near and slightly above the Coulomb barrier. Many important studies on ICF are available in the literature^{9, 10}, but their dependence on various input parameters motivated the ICF study. Hinde *et al.*¹³ suggested that the fusion suppression is almost proportional to the target charge Z_T . However, Rafiei *et al.*¹⁴ observed the non-dependency of the ICF probability with the target charge (Z_T). These studies suggest that more research is needed to establish a proper relationship between ICF and Z_T . Morgenstern *et al.*¹⁵ correlated the CF probability with the projectile-target mass asymmetry. The ICF probability increases linearly with increasing the product of the projectile and target charges $Z_p Z_T$ ¹⁶. A recent report on studies based on FRRD proposes that fusion suppression occurs due to projectile break-up threshold energy¹⁷. It is thus evident how various entrance channel parameters influence ICF reaction. Our objective in this current study is to investigate the behaviour of the ICF process by analyzing various entrance channel parameters that include mass-asymmetry (μ_{MA}), Coulomb factor ($Z_p Z_T$), deformation parameter (β_2), zeta parameter (ζ) and $Z_p Z_T \times \beta_2$. Our focus is on the FRRDs of evaporation residues that are produced in the $^{20}\text{Ne} + ^{159}\text{Tb}$ system at 8.2 MeV per nucleon energy. The measured FRRDs are analyzed in the framework of understanding different degrees of LMT associated with CF and/or ICF reaction products. From the present FRRD data analysis, the relative contribution due to different fusion components has been separated out. To achieve this goal, a thorough analysis of the aforementioned parameters and their impact on the ICF process has been conducted. As per our knowledge, it is the first time that FRRDs of evaporation residues have been measured and reported for the $^{20}\text{Ne} + ^{159}\text{Tb}$ system. The methodology undertaken in the current investigation is based on rigorous experimentation and data analysis. Great care has been taken to ensure the accuracy and reliability of our results. The findings of this study will provide valuable insights into the behaviour of this process and its potential applications in various fields. This paper is structured into four sections. Section 2 delves into the experimental details, while Section 3 analyses the measured FRRD data using code SRIM and interprets

the findings. The final section, Section 4, presents a summary and conclusions of the present work.

2 Experimental Procedures

The experiment was performed at the Variable Energy Cyclotron Centre (VECC), Kolkata, for FRRD measurement to disentangle different degrees of linear momentum transfer (LMT) using a ^{20}Ne beam on a ^{159}Tb target. The stack arrangement for FRRD measurements consists of a thin self-supporting ^{159}Tb target (abundance~100%) followed by a series of extremely thin (thickness ~ 71 - $95\mu\text{g}/\text{cm}^2$) Al-catcher foils. The self-supporting ^{159}Tb target of thickness $\sim 0.73\text{ mg}/\text{cm}^2$ and thin Al-catcher foils of variable thicknesses lying between 71 - $95\mu\text{g}/\text{cm}^2$ have been prepared by rolling machine and evaporation technique respectively at the target laboratory, VECC-Kolkata. The thickness of the target and each Al-catcher foil was determined by using the α -transmission method. The irradiation of the ^{159}Tb target, along with a stack of thin Al-catcher foils, have been performed using a ^{20}Ne -ion beam at energy ~ 8.2 MeV per nucleon in a specially designed vacuum chamber at VECC, Kolkata. A typical target-catcher foils arrangement used for the FRRD measurement is shown in Fig. 1.

The ^{159}Tb target faced the ^{20}Ne -ion beam followed by Al catcher foils for the present measurement. The irradiation of the stack has been carried out for ~ 21 hrs with beam current $\sim 34\text{nA}$. After the irradiation, the target-catcher assembly was removed from the scattering chamber, and activities induced in each irradiated Al catcher foil were individually recorded with the HPGe detector counting set-up. The reaction residues have been identified from their characteristic gammas in the spectrum. The evaporation residues populated via CF and/or ICF process are expected to be trapped at different catcher foil thicknesses, depending upon the degree of LMT associated with

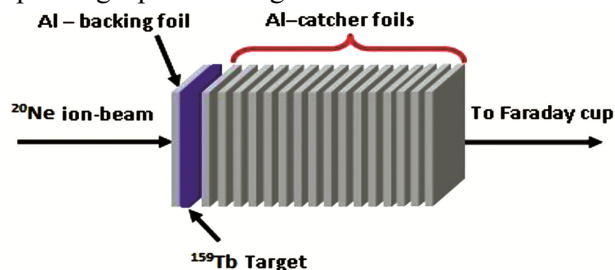


Fig. 1 — A typical stack foil arrangement consisting of a ^{159}Tb target followed by a series of thin Al-catcher foils used for FRRD measurement.

the mode of formation. The radioactivity induced in each catcher foil was recorded using a pre-calibrated high-resolution HPGe detector coupled to a PC-based data acquisition system equipped with Software MAESTRO¹⁸ at VECC-Kolkata. The γ -ray spectrum of each foil has been recorded at increasing times and has been shown in Fig. 2. The decay curve analysis has been done to ensure the production of the identified residues. The standard ^{152}Eu γ -ray source of known strength was used for the energy calibration and to determine the HPGe detector's efficiency.

3 Analysis and interpretation of data

The measurement of projected ranges of the residues in the stopping medium may give valuable information about LMT and hence the mechanism involved in the reaction. The degree of linear momentum associated with heavy recoiling residues formed as a result of CF and/or ICF processes has

been described by using the classical approach. In the $^{20}\text{Ne}+^{159}\text{Tb}$ system, ^{174}W (p4n), ^{175}Ta (α), ^{173}Ta ($\alpha 2n$), ^{172}Ta ($\alpha 3n$), ^{173}Hf (αpn), ^{164}Yb ($2\alpha p 6n$), ^{166}Tm ($3\alpha n$), ^{165}Tm ($3\alpha 2n$) and ^{163}Tm ($3\alpha 4n$) residues have populated. In order to obtain the LMT components involved in the reaction, the normalized yield of the evaporation residues in the catcher with their respective thickness has been measured at projectile energy ~ 8.2 MeV per nucleon. The FRRDs of evaporation residues ^{174}W (p4n), ^{175}Ta (α), ^{173}Ta ($\alpha 2n$), ^{172}Ta ($\alpha 3n$), ^{164}Yb ($2\alpha p 6n$) and ^{165}Tm ($3\alpha 2n$) have been reported¹⁹. Following the observations, herein a cross-sectional data and other details of the residues ^{173}Hf (pan), ^{166}Tm ($3\alpha n$), and ^{163}Tm ($3\alpha 4n$) completes the analysis for FRRDs measurements for $^{20}\text{Ne}+^{159}\text{Tb}$ system. The FRRD of evaporation residue ^{173}Hf is shown in Fig. 3 (a). It is evident from the figure the FRRD of residue ^{173}Hf shows a single

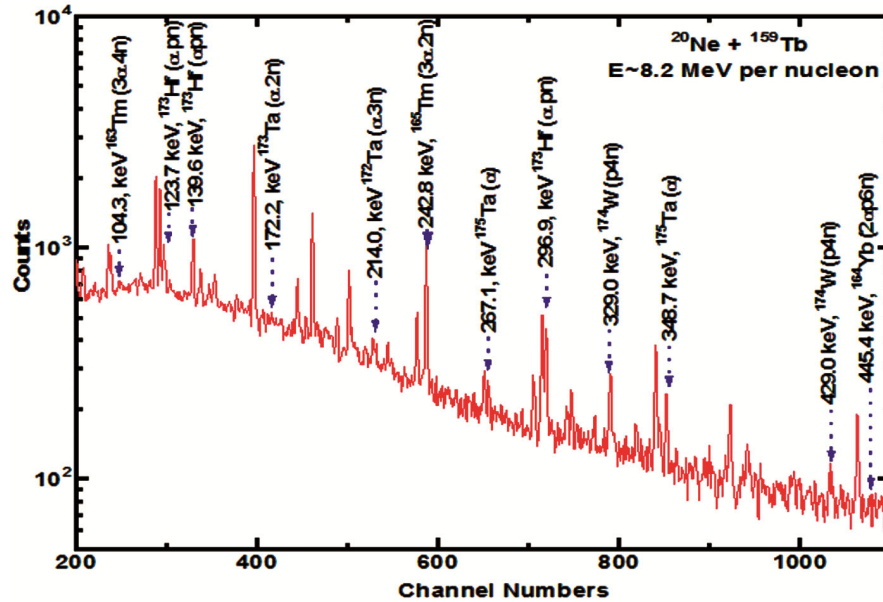


Fig. 2 — Typical γ -ray spectrum obtained for the $^{20}\text{Ne} + ^{159}\text{Tb}$ system at $E \approx 8.2$ MeV/nucleon.

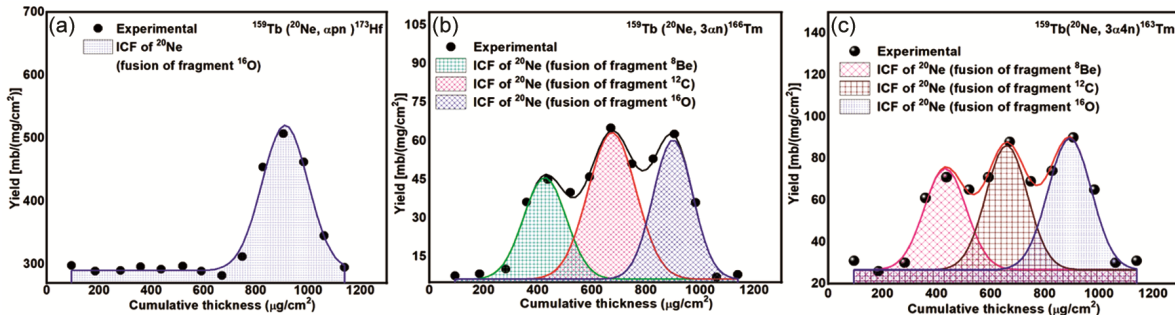


Fig. 3(a), (b), (c) — Figure shows FRRDs for the reaction products ^{173}Hf , ^{166}Tm and ^{163}Tm produced in the collision of ^{20}Ne on ^{159}Tb target at energy ~ 8.2 MeV per nucleon respectively.

Gaussian peak at cumulative depth $\sim 912 \mu\text{g}/\text{cm}^2$ which is due to ICF of projectile ^{20}Ne (fusion of fragment ^{16}O of the projectile ^{20}Ne which breaks up into ^{16}O and α particle) with ^{159}Tb target. Notably, no peak appears at a cumulative depth corresponding to full momentum transfer (CF process). The experimentally observed mean recoil range of $\sim 912 \mu\text{g}/\text{cm}^2$ deduced from FRRD agrees well with the theoretically calculated range of $\sim 916 \mu\text{g}/\text{cm}^2$ using code SRIM²⁰. It indicates that reaction product ^{173}Hf predominantly occurs through the ICF process.

For 3α -emitting channels, the recoil range distribution of the evaporation residues ^{166}Tm and ^{163}Tm shows more than two Gaussian peaks in Fig. 3 (b & c). As can be observed from Fig. 3(b), the deduced recoil range distribution for the residue ^{166}Tm may be convoluted into three Gaussian peaks at different cumulative depths $\sim 905 \mu\text{g}/\text{cm}^2$, $\sim 658 \mu\text{g}/\text{cm}^2$ and $\sim 432 \mu\text{g}/\text{cm}^2$, while in ^{163}Tm as shown in Fig. 3 (c), three Gaussian peaks are observed at ~ 903 , ~ 656 and $\sim 440 \mu\text{g}/\text{cm}^2$ indicating the presence of more than one LMT components. The observed mean recoil range of residue ^{166}Tm and ^{163}Tm at cumulative thickness ~ 905 & $903 \mu\text{g}/\text{cm}^2$ is due to ICF of ^{20}Ne (i.e. fusion of fragment ^{16}O as ^{20}Ne break-up into ^{16}O and α particle) with ^{159}Tb target, observed mean recoil ranges at cumulative thickness ~ 658 & $656 \mu\text{g}/\text{cm}^2$ is due to ICF of ^{20}Ne (i.e. fusion of fragment ^{12}C produced in the break-up of ^{20}Ne into ^{12}C and ^8Be) with ^{159}Tb target and the observed mean recoil range at thickness ~ 432 & $440 \mu\text{g}/\text{cm}^2$ is due to ICF of ^{20}Ne (i.e. fusion of fragment ^8Be as projectile ^{20}Ne in the break-up into fragments ^8Be and 3α) with ^{159}Tb target

has been observed. The reaction products ^{166}Tm and ^{163}Tm predominantly underwent the process of ICF is apparent with the absence of a peak corresponding to the CF process. The above descriptions indicate that peaks appearing at different cumulative thicknesses in the stopping medium are related to different degrees of LMT from the projectile to the target.

As discussed above, these peaks are associated with ICF of projectile ^{20}Ne (i.e. fusion of fragment ^{16}O , the fusion of fragment ^{12}C & fusion of fragment ^8Be) with the ^{159}Tb target. Observation of no peak at the CF recoil range indicates that no full LMT component is observed¹⁹ in residues ^{166}Tm and ^{163}Tm , and hence the given residues are predominantly produced through the ICF process. The experimentally measured most probable ranges $R_p(\text{exp})$ deduced from FRRD curves along with theoretical ranges $R_p(\text{theo})$ evaluated from code SRIM, for ICF components produced in the collision of ^{20}Ne beam on ^{159}Tb target, are listed in Table 1. As can be observed from Table 1, experimentally measured most probable ranges for ICF components agree well with theoretical values.

In the present manuscript, the relative contribution of ICF components has been deduced from the present FRRD analysis for $^{20}\text{Ne} + ^{159}\text{Tb}$ system at energy ~ 8.2 MeV per nucleon is listed in Table 2. The CF and ICF contributions can be computed by dividing the area of the corresponding peak by the total area under the FRRD curve. The residue ^{173}Hf is populated via ICF, and the ICF contributions of the projectile ^{20}Ne by the fusion of the fragment ^{16}O with the target are found to be 100%, while no CF contribution has been obtained.

Table 1 — The experimentally measured recoil ranges $R_p(\text{exp})$ deduced from FRRD curves and theoretically calculated ranges $R_p(\text{theo})$ for CF and/or ICF reaction products produced in the interaction of ^{20}Ne with ^{159}Tb target at energy ~ 8.2 MeV per nucleon.

Residues	$R_p(\text{exp})$	$R_p(\text{theo})$	$R_p(\text{exp})$	$R_p(\text{theo})$	$R_p(\text{exp})$	$R_p(\text{theo})$	$R_p(\text{exp})$	$R_p(\text{theo})$
	$[\mu\text{g}/\text{cm}^2]$							
	CF of ^{20}Ne	CF of ^{20}Ne	ICF of ^{16}O	ICF of ^{16}O	ICF of ^{12}C	ICF of ^{12}C	ICF of ^8Be	ICF of ^8Be
^{173}Hf (αpn)	---	---	912 ± 87	916	---	---	---	---
^{166}Tm ($3\alpha\text{n}$)	---	---	905 ± 73	916	658 ± 88	651	432 ± 78	443
^{163}Tm ($3\alpha 4\text{n}$)	---	---	903 ± 80	916	656 ± 76	651	440 ± 77	443

Table 2 — The measured relative contribution of CF and/or ICF of the reaction products produced in the interaction of ^{20}Ne with ^{159}Tb target at energy ~ 8.2 MeV per nucleon.

Residue	ICF of ^{20}Ne			
	CF of ^{20}Ne	Fusion of fragment ^{16}O	Fusion of fragment ^{12}C	Fusion of fragment ^8Be
^{173}Hf (αpn)	--	100%	--	--
^{166}Tm ($3\alpha\text{n}$)	--	32%	42%	26%
^{163}Tm ($3\alpha 4\text{n}$)	--	38%	34%	28%

In the case of residues ^{166}Tm & ^{163}Tm , the relative ICF contribution of fragments from ^{16}O , ^{12}C , and ^8Be is found to be 32%, 42%, 26% and 38%, 34%, and 28%, respectively.

3 (i) Entrance Channel Parameter Effect on ICF

In order to attain a more comprehensive comprehension of the intricate dynamics implicated in the ICF reaction, a systematic investigation was undertaken to scrutinize the potential impact of various entrance channel parameters, namely μ_{MA} , $Z_p Z_T$, β_2 and $Z_p Z_T \times \beta_2$. To comprehensively investigate the impact of entrance channel parameters on the current dataset, a thorough analysis of the probability function (F_{ICF}) has been undertaken for the $^{20}\text{Ne} + ^{159}\text{Tb}$. The F_{ICF} is evaluated by using the relation as given below;

$$F_{\text{ICF}} (\%) = \frac{\Sigma \sigma_{\text{ICF}}}{\Sigma \sigma_{\text{CF}} + \Sigma \sigma_{\text{ICF}}} \times 100$$

where $\Sigma \sigma_{\text{CF}}$ and $\Sigma \sigma_{\text{ICF}}$ are the sums of CF and ICF channel cross-sections.

Morgenstern *et al.*¹⁵ showed that ICF contribution is more in the mass-asymmetric systems and less in the mass-symmetric system. Taking this into account, the ICF fraction for the present system $^{20}\text{Ne} + ^{159}\text{Tb}$ has been compared with literature data at fixed relative velocity as a function of entrance channel mass-asymmetry (μ_{MA}). The relative velocity is defined as;

$$V_{\text{rel}} = \sqrt{\frac{2(E_{\text{CM}} - V_B)}{\mu}}$$

Where E_{CM} is projectile energy, V_B is the Coulomb barrier of the system in the centre of the mass frame, and μ is the reduced mass of the system. The relative velocity (V_{rel}) of the nucleons in the compound nucleus has been widely used as a normalization factor to compare the ICF fractions of the different systems. The ICF fraction for the present system $^{20}\text{Ne} + ^{159}\text{Tb}$, along with previously measured systems $^{20}\text{Ne} + ^{51}\text{V}$ ²¹, $^{20}\text{Ne} + ^{59}\text{Co}$ ²² and $^{20}\text{Ne} + ^{165}\text{Ho}$ ²³ from the literature as a function of mass-asymmetry [$A_T / (A_T + A_p)$] at a constant relative velocity ($V_{\text{rel}} = 0.09c$) have been estimated and plotted as a function of mass-asymmetry and is shown in Fig. 4. As can be observed from Fig. 4 that ICF fraction increases with mass-asymmetry of different projectile-target combinations and in general ICF probability is more in the mass-asymmetric system than mass-symmetric systems.

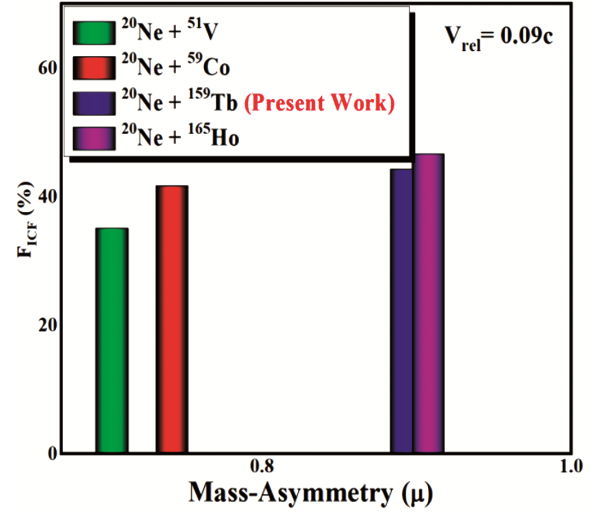


Fig. 4 — Figure shows the comparison of F_{ICF} with mass-asymmetry for present system $^{20}\text{Ne} + ^{159}\text{Tb}$ along with literature data²¹⁻²³ at fixed value of $V_{\text{rel}} = 0.09c$.

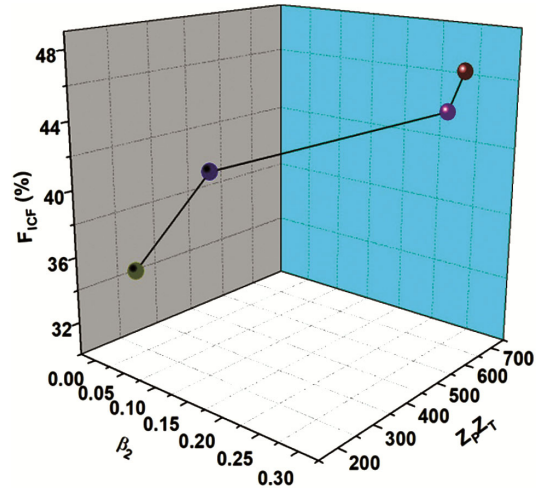


Fig. 5 — Figure shows the comparison of F_{ICF} with β_2 and $Z_p Z_T$ for systems $^{20}\text{Ne} + ^{51}\text{V}$ ²¹, $^{20}\text{Ne} + ^{59}\text{Co}$ ²², $^{20}\text{Ne} + ^{159}\text{Tb}$ & $^{20}\text{Ne} + ^{165}\text{Ho}$ ²³ (in points from left to right, respectively) at a fixed value of $V_{\text{rel}} = 0.09c$.

In order to see the effect of $Z_p Z_T$ and β_2 on ICF reaction dynamics, ICF fraction (F_{ICF}) from FRRD data has been deduced for the present system $^{20}\text{Ne} + ^{159}\text{Tb}$ along with other systems obtained from literature²¹⁻²³ at fixed relative velocity ($V_{\text{rel}} = 0.09c$). Data was thereby plotted as a function of $Z_p Z_T$ and β_2 is shown in Fig. 5. It has been observed from Fig. 5 that there is approximately a linear growth in incomplete fusion fraction (F_{ICF}) with increasing $Z_p Z_T$ and β_2 at constant $V_{\text{rel}} = 0.09c$. The solid line connecting the experimental data points is to guide the eye. This clearly indicates that the $Z_p Z_T$ and β_2

affect the ICF reaction dynamics for the same projectile (^{20}Ne) with different targets. It is also evident from Fig. 5 that the F_{ICF} values deduced for the reaction with target ^{159}Tb have a higher value than those for the targets ^{51}V , ^{59}Co and less than those for the target ^{165}Ho . The findings, therefore, clearly indicate ICF fraction being higher in a more deformed target than in a lesser one.

An attempt has been made to see the combined effect of μ_{MA} and $Z_{\text{P}}Z_{\text{T}}$, the ICF fraction (F_{ICF}) studied as a function of the zeta parameter (ζ) in this study. The ζ parameter is defined as;

$$\zeta = Z_{\text{P}}Z_{\text{T}}\sqrt{\mu} = Z_{\text{P}}Z_{\text{T}}\sqrt{\frac{A_{\text{P}}A_{\text{T}}}{A_{\text{P}}+A_{\text{T}}}}$$

$$= Z_{\text{P}}Z_{\text{T}}\sqrt{A_{\text{P}}\times\mu_{\text{MA}}}$$

where reduced mass, $\mu = \frac{A_{\text{P}}A_{\text{T}}}{A_{\text{P}}+A_{\text{T}}}$

and mass-asymmetry, $\mu_{\text{MA}} = \frac{A_{\text{T}}}{A_{\text{P}}+A_{\text{T}}}$

The measured values of ICF-fraction for the present system $^{20}\text{Ne} + ^{159}\text{Tb}$, along with the other systems from the literature²¹⁻²³, have been plotted as a function of ζ at $V_{\text{rel}} = 0.09c$ and is shown in Fig. 6. It is clear from Fig. 6 that ICF fraction increases with zeta parameter (ζ) for a same projectile (^{20}Ne) with different targets. It is important to mention that it contains the information on μ_{MA} and $Z_{\text{P}}Z_{\text{T}}$; hence, it alone can explain the dependence of ICF on these two mentioned entrance channel parameters.

The combined effect of charges in terms of $Z_{\text{P}}Z_{\text{T}}$ and their structural effect in terms of β_2 have been investigated for $^{20}\text{Ne} + ^{159}\text{Tb}$ system.

In this regard, a graph between F_{ICF} vs. $Z_{\text{P}}Z_{\text{T}}\times\beta_2$ has been plotted. For the present system $^{20}\text{Ne} + ^{159}\text{Tb}$ along with other systems²¹⁻²³, it has been observed from Fig. 7 that for β_2 ranging from 0.021 (for ^{51}V) to 0.284 (for ^{159}Tb) and $Z_{\text{P}}Z_{\text{T}}$ from 230 (for ^{51}V) to 670 (for ^{159}Tb) F_{ICF} changes from 35% to 46% almost linearly. It can be concluded that as an effect of an increase in the charges of interacting nuclei and deformity of targets, the incomplete fusion increases almost linearly.

4 Summary and Conclusions

The investigation of forward recoil range distribution associated with fusion and break-up fusion populating three different radio-nuclides ^{173}Hf , ^{166}Tm and ^{163}Tm in the collision of ^{20}Ne -ion beam on

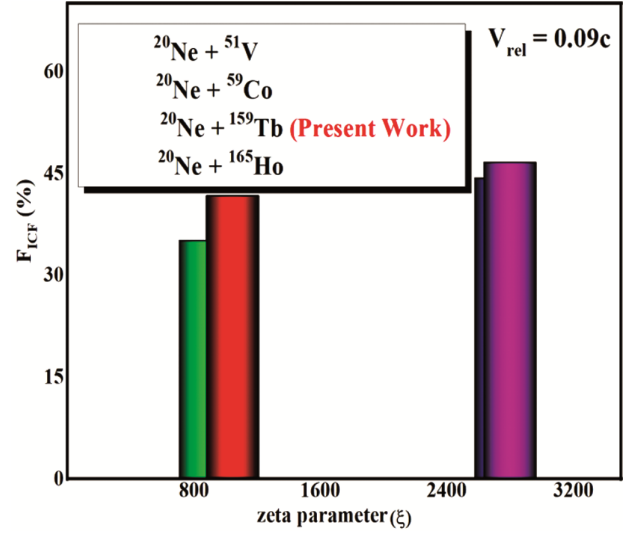


Fig. 6 — Figure shows the comparison of F_{ICF} with the ζ parameter for a fixed value of $V_{\text{rel}} = 0.09c$.

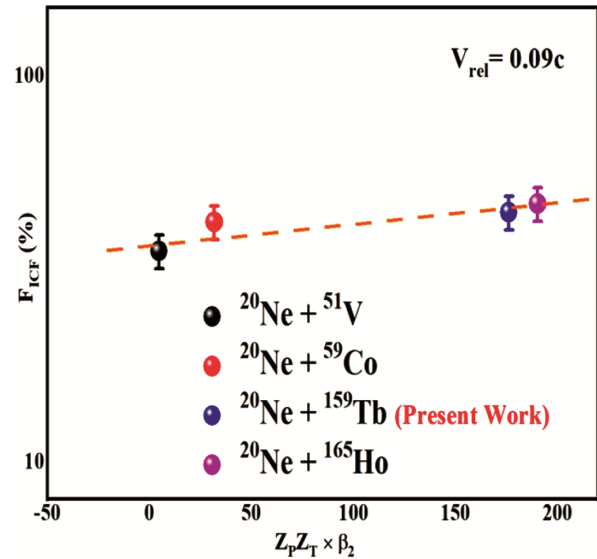


Fig. 7 — Figure shows the comparison of F_{ICF} with $Z_{\text{P}}Z_{\text{T}}\times\beta_2$ for $^{20}\text{Ne} + ^{159}\text{Tb}$ system at a fixed value of $V_{\text{rel}} = 0.09c$.

^{159}Tb target have been carried out at ~ 8.2 MeV per nucleon energy. The evaporation residues ^{173}Hf , ^{166}Tm and ^{163}Tm involving the α -particle (s) strongly reveal the presence of partial LMT components. The forward recoil range analysis is accomplished in the framework of code SRIM. It is observed that the fractional LMT, the ICF products traverse relatively shorter depth in the stopping medium as compared to CF products. The partial LMT components associated with break-up of the projectile ^{20}Ne into $^{16}\text{O} + ^4\text{He}$ (α) and/or $^{12}\text{C} + ^8\text{Be}$ (2α) and/or $^8\text{Be} + ^{12}\text{C}$ (3α) is observed. The experimentally measured recoil ranges

R_p (exp.) is deduced from the fitting of experimentally FRRD data points. The experimentally measured recoil ranges in α -emission products have been compared with theoretically calculated ranges R_p (theo) by using code SRIM is found to be in good agreement. In the present paper, the relative contribution of fusion of ^{20}Ne , ^{16}O , ^{12}C and ^8Be have also been separated out. To study the effects of entrance channel parameter on ICF dynamics, the ICF fraction (F_{ICF}) for the present system and systems from literature²¹⁻²³ has been calculated at a fixed value of $V_{\text{rel}} = 0.09c$ and plotted against μ_{MA} , $Z_p Z_T$, β_2 , ζ and $Z_p Z_T \times \beta_2$. From the result, it has been found that the ICF cross-section increases with the increase in μ_{MA} for different systems. The $F_{\text{ICF}}(\%)$ values for various systems as a function of μ_{MA} depict that F_{ICF} is more for mass-asymmetric systems than for mass-symmetric systems. It has also been observed that the higher the value of the Coulomb factor ($Z_p Z_T$), the more the ICF fraction. This is due to projectile break-up probability being higher at a larger value of the Coulomb factor. Additionally, the value of target deformation for target ^{159}Tb is more than ^{51}V , ^{59}Co but less than ^{165}Ho consequently, as opposed to ICF fraction which is more for ^{159}Tb than ^{51}V , ^{59}Co but less than ^{165}Ho . The combined effect of the coulomb factor and deformation in terms of $Z_p Z_T \times \beta_2$ has suggested that role of ICF is dependent on the charges in terms of the amount and their distribution of interacting nuclei. From the ζ systematic, it has been found that F_{ICF} demonstrates a linear increase upon considering various projectile-target combinations. This observation is of great significance as the parameter ζ incorporates valuable information regarding the mass and charge of the projectile and target in terms of μ_{MA} and $Z_p Z_T$. This knowledge is essential for the development of theoretical models pertaining to the dynamics of fusion reactions, particularly in low-energy nuclear reactions.

Acknowledgement

The authors are thankful to the Director, VECC-Kolkata, for providing all the necessary experimental facilities to carry out the research experiment. One of the authors (R. Ali) acknowledges the funding support to UGC-DAE Consortium for Scientific Research, Kolkata Centre.

References

- 1 Back B B, Esbensen H, Jiang C L & Rehm K E, *Rev Modern Phys*, 86 (2014) 317.
- 2 Bock R, Chu Y T, Dakowski M, Gobbi A, Grosse E, Olmi A, Sann H, Schwalm D, Lynen U, Müller W, Bjørnholm S, Esbensen H, Wölfli W & Morenzoni E, *Nucl Phys A*, 388 (1982) 334.
- 3 Toke J, Bock R, Dai G X, Gobbi A, Gralla S, Hildenbrand K D, Kuzminski J, Müller W F J, Olmi A, Stelzer H, Back B B & Bjørnholm S, *Nucl Phys A*, 440 (1985) 327.
- 4 Britt H C & Quinton A R, *Phys Rev*, 124 (1961) 877.
- 5 Inamura T, Ishihara M, Fukuda T, Shimoda T & Hiruta H, *Phys Lett B*, 68 (1977) 51.
- 6 Galin J, Gatty B, Guerreau D, Rousset C, Scholtthauer-Voos U C & Tarrago X, *Phys Rev C*, 9 (1974) 1126.
- 7 Parker D J, Hodgson J J & Asher J, *Phys Rev C*, 39 (1989) 2256.
- 8 Gomes P R S, Padron I, Rodriguez M D, Marti G V, Anjos R M, Lubian J, Veiga R, Liguori N R, Crema E, Added N, Chamon LC, Fernandez N J O, Capurro O A, Pacheco A J, Testoni J E, Abriola D, Arazi A, Ramirez M & Hussein M S, *Phys Lett B*, 601 (2004) 20.
- 9 Singh D, Linda Sneha B, Giri Pankaj K, Mahato Amritraj, Tripathi R, Kumar H, Tali Suhail A, Parashari Siddharth, Ali Asif, Dubey Rakesh, Ansari M Afzal, Kumar R, Muralithar S & Singh R P, *Phys Rev C*, 97 (2018) 064610.
- 10 Kumar S, Giri Pankaj K, Kumar R, Yadav Abhishek, Ali Rahbar, Appannababu S, Agarwal Avinash, Mukherjee S, Singh Pushpendra P, Sharma Vijay R, Singh BP & Dutt Sunil, *J Phys G: Nucl Part Phys*, 49 (2022) 105103.
- 11 Udagawa T & Tamura T, *Phys Rev Lett*, 45 (1980) 1311.
- 12 Wilczynski J, Siwek-Wilezynaska K, Van-Driel J, Gonggrijp S, Hageman D C J M, Janssens R V F, Lukasiak J, Siemssen R H & Van der Werf S Y, *Nucl Phys A*, 373 (1982) 109.
- 13 Hinde D J, Dasgupta M, Fulton B R, Morton C, Wooliscroft R J, Berriman A C & Hagino K, *Phys Rev Lett*, 89 (2002) 27701.
- 14 Rafiei R, Rietz R du, Luong D H, Hinde D J, Dasgupta M, Evers M & Diaz-Torres A, *Phys Rev C*, 81 (2010) 024601.
- 15 Morgenstern H, Bohne W, Galster W, Grabisch K & Kyanowski A, *Phys Rev Lett*, 52 (1984) 1104.
- 16 Tali S A, Kumar H, Ansari M A, Ali A, Singh D, Ali R, Giri P K, Linda S B, Parashari S, Kumar R, Singh R P & Muralithar S, *Nucl Phys A*, 970 (2018) 208.
- 17 Kumar H, Tali S A, Ansari M A, Singh D, Ali Rahbar, Ali Asif, Parashari S, Giri, Pankaj K, Linda S B, Kumar R, Singh R P & Muralithar S, *Phys Rev C*, 99 (2019) 034610.
- 18 MAESTRO; Data acquisition and analysis software coupled with E G & G ORTEC Hardware, USA.
- 19 Khan Mohd A & Ali Rahbar, *Int J Sci Res*, (2020) 26.
- 20 Ziegler J F, *SRIM08*, <http://www.srim.org/>, *the Stopping Power and Range of Ions in Matter*, 2008.
- 21 Sabir Ali, Tauseef Ahmad, Kamal Kumar, Rizvi I A, Agarwal A, Ghugre S S, Sinha A K & Chaubey A K, *EPJ Web Conf*, 86 (2015) 00002.
- 22 Singh D, Ali R, Ansari M A, Tomar B S, Rashid M H, Guin R & Das S K, *Phys Rev C*, 83 (2011) 054604.
- 23 Singh D, Ali Rahbar, Ansari M A, Tomar B S, Rashid M H, Guin R & Das S K, *Nucl Phys A*, 879 (2012) 107.